IV Conferencia Panamericana de END
Buenos Aires – Octubre 2007

Results of on-orbit testing of an extra-vehicular infrared camera inspection System

Patricia A. Howell and K. Elliott Cramer
Nondestructive Evaluation Sciences Branch
Mail Stop 231, 3B E. Taylor Rd
NASA Langley Research Center
Hampton, VA 23681-2199, USA
757-864-4786
757-864-4914 (fax)
p.a.howell@nasa.gov

Abstract

This paper will discuss an infrared camera inspection system that has been developed to allow astronauts to demonstrate the ability to inspect reinforced carbon-carbon (RCC) components on the space shuttle as part of extra-vehicular activities (EVA) while in orbit. Presented will be the performance of the EVA camera system coupled with solar heating for inspection of damaged RCC specimens and NDE standards. The data presented was acquired during space shuttle flights STS-121 and STS-115 as well during a staged EVA from the ISS. The EVA camera system was able to detect flat-bottom holes as small as 2.54cm in diameter with 25% material loss. Results obtained are shown to be comparable to ground-based thermal inspections performed in the laboratory using the same camera and simulated solar heating. Data on both the time history of the specimen temperature and the ability of the inspection system to image defects due to impact will likewise be presented.

1. Introduction

After the Shuttle Columbia accident, several new tools and inspection procedures were developed to ensure the integrity of the Shuttle's thermal protection system prior to re-entry. The development of a nondestructive, noncontacting, handheld EVA inspection tool was proposed as an additional focused inspection technique. The goal of this tool is to provide information regarding the presence of subsurface damage to the reinforced carbon-carbon (RCC) material of the wing leading edge of the Shuttle. Thermography had been used extensively during ground tests to quantify impact-induced damage to the orbiter's wing leading edge material as part of NASA's Return to Flight program[(1), (2)].

Based on the success of thermal NDE for ground inspections of Shuttle RCC, a handheld infrared camera was developed to test the ability of thermography to detect possible damage during a mission. To save on weight and power requirements, a commercially available microbolometer was modified to withstand the space environment, with special consideration given to the constraints of using the camera

during an EVA. This instrument is a compact, low-mass, low-power solution for TPS inspection.

To detect underlying RCC damage with infrared thermography, a thermal gradient through the RCC panel must exist. On the ground, inspectors use large flash lamps to generate a thermal gradient. The power, weight and cost requirements for space-qualifying flash lamps for the on-orbit system made their development impractical. Rather than packaging a flash lamp for space, the EVA IR Camera project team conducted a series of tests on the ground to demonstrate that sunlight and shadowing could be used to generate an adequate thermal gradient through the RCC panels. This significantly simplifies the development tasks and reduces project costs. However, it also increases operational complexity, since crewmembers are constrained to inspecting the RCC in sunlight.

This paper delineates the major differences in boundary conditions that effect the measurements between the thermography inspections conducted on the ground versus the conditions and limitations inherent on-orbit, and how those differences were managed to provide a potential inspection capability during a mission. Processing algorithms were developed to correct for the motion between the object and the camera. Since a microbolometer has significant associated noise, an algorithm was added to the processing that spatially smoothes the data while maintaining information along defect edges. This algorithm is shown to substantially improve the image quality for this detector. The boundary conditions existing during orbit for both heating and cooling are significantly different than those existing for ground inspections. These differences and their effect on the inspection technique are discussed.

2. Hardware and Measurement Technique Development

2.1 Camera Hardware

The thermal NDE system used for ground inspections consists of a high resolution, high speed cooled detector. The significant limitations of available resources during space missions, such as weight and power, were defining parameters in the selection of the infrared camera. Further, budget and time considerations led to a decision to modify a COTS camera. This camera had to be capable of collecting and storing a series of images to provide the necessary data for NDE processing. Details of the camera modifications necessary to transition the COTS camera to space flight hardware are discussed in Gazarik, *et. al.* [3]. A photograph of the final camera system modified for on-orbit use is shown in Figure 1.

An uncooled microbolometer camera was chosen in order to minimize the system weight and required power. While cooled detector cameras provide significantly better signal-to-noise, the microbolometer provides sufficient signal-to-noise for detecting delaminations of the size and depth of interest, with lower weight and power consumption. The camera has a spectral range of 7.5 to 13μm with a 320 x 240 pixel focal plane array. The field of view is 24° x 18° with a minimum focus distance of 0.3m. It has a thermal sensitivity of 0.06°C at ambient and can collect and store up to

600 frames of 14 bit integer data to built-in RAM at frame rates varying from 0.6 hertz to 30 hertz.

Figure 1. Photograph of EVA IR Camera Flight Unit. The camera consists of two major components: the camera body with the germanium infrared detector, battery, memory, and flash drive, and the Remote Control Unit (RCU) containing the LCD screen and control buttons.

2.2 Feasibility Testing

To save development time and costs as well as system weight and required energy, the feasibility of detecting sub-surface damage under on-orbit solar conditions was explored by imaging damaged RCC samples using quartz lamps to simulate the expected solar flux. The maximum expected absorbed solar flux on-orbit is approximately 1100W/m^2. Two quartz lamps were used in a laboratory environment (ambient temperature and pressure) to simulate expected solar flux. By measuring the temperature profile in RCC and knowing the material properties of RCC (thermal conductivity), the lamp power settings were calibrated to solar flux levels. In addition, the measured temperature profiles were compared to a model simulation of RCC and found to be in good agreement. Figure 2 shows the laboratory test setup.

2.3 Thermal Boundary Conditions and Operational Considerations On-orbit

Significant changes to the data acquisition and processing approach were necessary to transition the ground system to an on-orbit inspection system. The thermal boundary conditions on the RCC are significantly different, with no convective heat losses from the structure, but significant radiative heat transfer possible. Additionally, significant heat conduction across a delamination is possible for ground inspections however in the vacuum of space there is no air to conduct heat across the gap.

Operationally, issues such as focus, frame rate acquisition time, issues of uneven heating and correction for the motion between the astronaut and the test article were investigated. To test these changes in the operational system, a set of seven RCC panels were obtained and impacted with varying velocities of SOFI (Spray-On Foam Insulation) foam to create samples with varying degrees of damage.

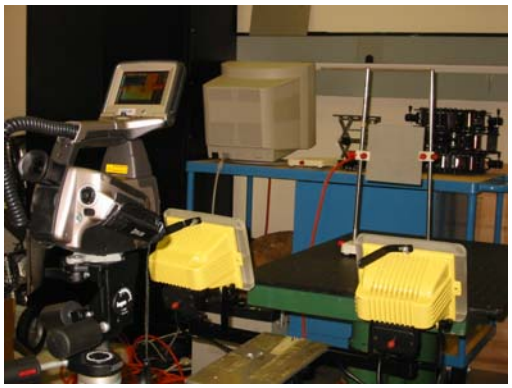

Figure 2. Laboratory test setup simulating solar flux conditions on RCC.

2.4 Impact Panel Descriptions

Seven samples approximately 15 cm wide x 15 cm high of RCC material were impacted with SOFI foam as shown in Figure 3. All seven samples were cut from a previously-flown section of RCC to provide samples with surface emissivity variations as seen on flight panels. The samples were held in a metal frame around the edge to allow the RCC to flex upon impact. The edges of the samples were cushioned from the metal frame with pliable putty to allow further sample motion. The RCC was impacted with SOFI foam that measured 2.5 cm x 2.5 cm cross section and was 5 cm long with a weight of 2 grams. The panels were impacted at speeds of approximately 610 m/s. Multiple impact events were conducted to create samples with more significant damage.

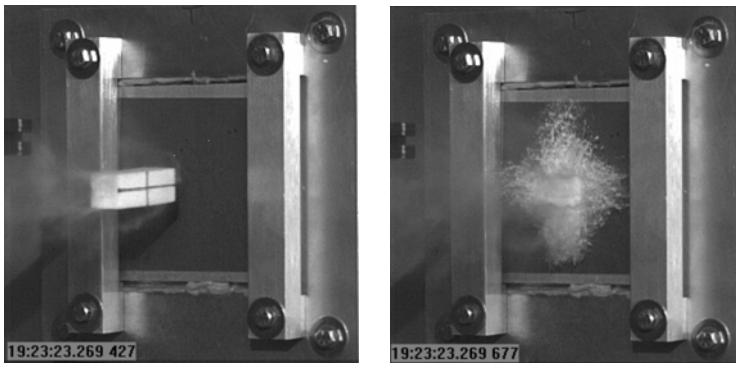

Figure 3. Photographs of foam impact on RCC panels. Left-hand image shows block of foam just prior to impact. Right-hand side shows foam immediately after impact.

These seven impact panels provided samples with a range of realistic delaminations to be used for technique development (from 1.25 cm. in diameter to 11.25 cm. x 13.75 cm.). The samples were characterized with ground-based flash thermography, with both active and simulated solar heating, and with both the ground-based IR camera and a commercial version of the microbolometer camera chosen for the orbital IR camera.

2.5 Input Heat Flux

One of the requirements of transitioning the NDE technique to an orbital system is the adaptation of the input heat flux for in-space operations. For the thermal system used for ground RCC tests, a short flash of heat is delivered to the front surface of the sample via two 4800 J xenon flash lamps. The infrared data is acquired during the cool-down phase. Reliance on solar energy to provide the input heat flux results in a much slower application of heat. Quantitative data reduction techniques that are used for RCC inspection require a time-varying thermal contrast between a flawed and an unflawed material. On-orbit, this condition is best achieved by data acquisition at the onset of solar heating or at the end of solar heating phase. Rather than relying on the orbital cycle to set the timing of the solar heating cycle, blocking the sunlight controls the initiation and end of solar heat during data collection. Ground-based experiments showed the feasibility of this approach both from a crew operations perspective as well as a data analysis perspective. For this test, two RCC specimens with known defects were placed under solar heating conditions. The first sample measured approximately 5 cm x 15 cm and contained three full-width defects of various depths. The second sample was approximately 15 cm x 15 cm and contained numerous flat-bottom holes of various depths and diameters. A photograph of these samples is shown in
Figure 4. NDE results of data collected under solar conditions on RCC both with and without shading are shown in Figure 5.

(A) (B)

Figure 4. Photograph of (A) front of samples and (B) back of RCC samples used for testing of thermal technique using solar heating.

2.6 Data analysis

The data analysis performed on the thermal data consisted of Principle Component Analysis (PCA) and anisotropic diffusion. PCA is an algorithm based on decomposition of the thermal data into its principle components. Singular value decomposition is a routine used to find the singular values and corresponding eigenvectors of a matrix. Since thermal NDE signals are well-behaved and slowly decaying waveforms, the spatial variations of the entire data set is usually contained in the first and second

eigenvectors and accounts for most of the data variance. PCA analyses were used routinely on the flash thermography conducted for ground inspections, and is discussed in greater detail elsewhere [(4)-(8)]. It was found that PCA also works well for the longer heat pulse input flux condition, using approximately the first 10 seconds of data immediately after shadowing of the sample.

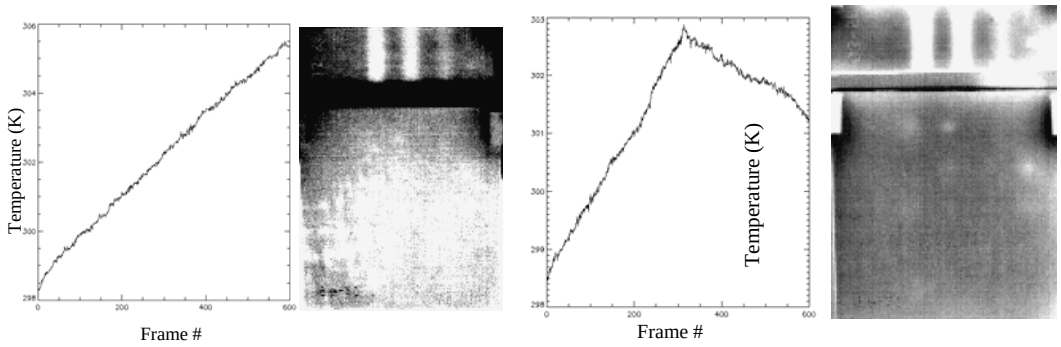

(A) (B)

Figure 5. (A) Processed thermal data on Shuttle RCC under solar conditions with no shading and (B) with shading

Anisotropic diffusion is a data processing technique that has been shown to enhance the contrast between damaged and undamaged regions in thermal images[(8)]. The technique has been shown to significantly reduce spatial image noise while maintaining defect contrast and preserving the important features of a flaw[(9)]. This is accomplished by a convolution of the data with a function containing a diffusion parameter. This parameter is high in regions of low gradients in image intensity and low in regions of high discontinuities in image intensity, as is the case near defect edges. For this data, the algorithm was applied to each frame of the data collected to remove spatial noise from the microbolometer data while maintaining any signal due to a delamination. Application of this algorithm resulted in a significant improvement in signal-to-noise of the final post-processed data, as seen qualitatively below in Figure 6.

2.7 Frame rate

To minimize transfer time from camera memory to the internal compact flash card, minimizing the number of frames of data collected is critical. Reducing the number of frames stored can be accomplished by decreasing the frame rate or by decreasing the amount of time data is collected. Operationally, the crew must coordinate the start of data collection with the application of a shadowing source during the sequence. For the flight experiment, this parameter was set at 60 seconds to ensure ample time for collection of the 10 second window after the initiation of shading.

Data was collected on an impact panel and subsampled to obtain different effective frame rates. After applying the anisotropic diffusion algorithm and PCA during the first ten seconds after initiation of shading, a signal-to-noise analysis was performed to determine the loss in signal due to decreasing the frame rate. The signal-to-noise is

defined as the difference between the base material response and the flaw signal divided by the standard deviation of the base material.

As seen in the Table 1 below, a 30% loss in signal-to-noise occurs when reducing the frame rate to 1 Hz. For the DTO, data was collected at 5 Hz for 60 seconds.

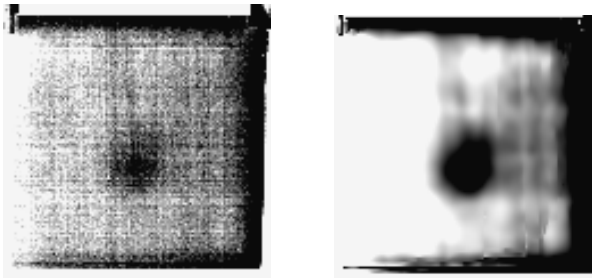

Figure 6. Post-processed microbolometer data, solar heating (A) without anisotropic diffusion, and (B) with Anisotropic Diffusion algorithm applied.

Table 1. Comparison of Signal-to-noise for various data collection rates

Signal to Noise calculated for impacted specimen				
Reduction parameters: Frequency of acquisition, start and stop channels	Signal	Standard Deviation Base Response	Signal to Noise	% Loss from 15 hz
15 Hz – 310,460	0.50	0.09	5.5	X
5 Hz - 104,154	0.50	0.09	5.5	0%
1 Hz – 21,31	0.39	0.10	3.9	29%
0.5 Hz – 10,15	0.34	0.10	3.4	38%
0.5 Hz – 11,16	0.37	0.10	3.6	34%

2.8 Radiation losses

Ground based thermographic inspection typically ignores radiation losses because these are small compared to the effects of convection. Performing thermography in a vacuum requires that losses due to radiation be included. A finite element simulation of the specimen with radiative heat transfer and a periodically applied heat flux to the front, and with continuous radiative heat transfer into fixed temperature at both the front and back surfaces was performed. A delamination was placed at the center plane of the specimen, with a radius-to-thickness ratio of 4:1. To reduce the computational time required for the simulation, the simulation was performed in cylindrical coordinates, approximating a circular delamination. For the simulations reported here, the back surface was assumed to always radiate into 270^{o}K and the front surface to radiate into either 10^{o}K or 170^{o}K. Simulations were also performed with incident fluxes of 1.1 Kwatt/meter^2 and 0.55 Kwatt/meter^2. For all cases considered here, the incident

flux is applied for the first half of a 90 minute cycle. All simulations assume an initial temperature of the entire specimen is 290^{o}K, with two full cycles of simulation before beginning to record the results. This was found to give results that were independent of the initial condition.

The time history of the temperature at a point far from the delamination is shown in Figure 7. The time in the figure is set to be zero at the beginning of a cycle. The simulation indicates the temperature increases at the beginning of the cycle as the incident flux is applied. During the application of the incident flux, the temperature increases at a decreasing rate, asymptotically approaching a temperature that is determined by the point when the incident flux would be equal to the radiative heat transfer. This is seen in the figure where the case of radiative heat transfer into 170^{o}K approaches a slightly higher temperature than for radiative heat transfer into 10^{o}K.

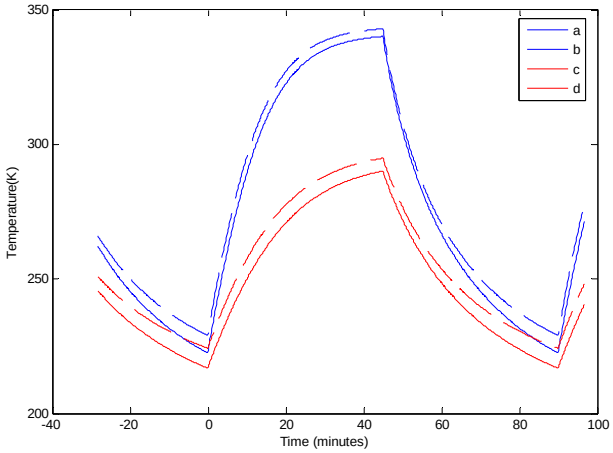

Figure 7. Results of simulation of thermal response of specimen radiating into two different temperatures and with two different surface fluxes.

3. Flight Results

Two major flight test objectives were identified. The first objective was to verify the operational inspection technique, and obtain measurements of the temperature profile of RCC under on-orbit solar heating conditions. Data from these measurements would be compared to wing leading edge temperature predictions and to estimate the boundary conditions on the RCC important to a NDE inspection. These parameters are required to predict damage detection limits. The second objective was to illustrate the effectiveness of the NDE technique under orbital conditions, validating the ground predictions for the on-orbit system.

3.1 Objective #1

The first flight test objective was to obtain wing leading edge (WLE) temperature data during orbit for comparison to wing leading edge temperature predictions and estimate the thermal boundary conditions on the RCC important to the NDE inspection.

Two 20-second thermal movie segments of the starboard WLE were obtained on STS-121. One movie segment was taken just after egress from the airlock, and the other toward the end of the EVA. Constraints of EVA timeline planning were the primary driver to this schedule. Both of these thermal movie segments were taken at approximately the same relative point in the orbital day/night sequence – approximately 5 minutes prior to orbital sunrise as shown below in Figure 8.

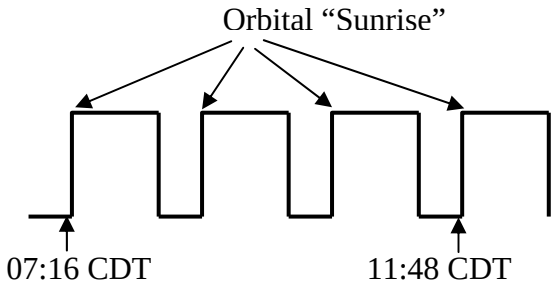

Figure 8. Graphic illustrating the periodic thermal solar load on the RCC during orbit overlaid with the times data was taken on the Shuttle wing leading edge with the EVA IR Camera on STS-121.

Because the purpose of this objective was to obtain WLE temperatures over a large span of the wing RCC panels, the astronaut was positioned approximately 6 meters from the wing. During an actual inspection, the proposed operational concept is to position the astronaut 1 to 2 meters away from the wing panel of interest. This distance is determined by the defect size of interest and the spatial resolution of the camera optics.

Figure 9 shows that for a region of interest over a representative RCC panel on the wing of the Shuttle and for a region over the white Felt Reusable Surface Insulation (FRSI) acreage region of the wing, the temperature has reached equilibrium in both regions during the nighttime cycle. The RCC is holding at a stable -44^{o}C and the FRSI is approximately 4^{o} colder at -48^{o}C. Assuming the FRSI to be a thermal insulator, it is possible to approximate the background temperature for the radiative heat loss to space as -48^{o}C. The first infrared movie taken at 07:16 CDT July 15, 2006 was used in Figure 9. The second movie of the WLE taken 4.5 hours later, of the same section of the wing, had similar results, although the temperature of the FRSI was as much as 5^{o}C colder than the previous movie sequence recorded. The difference in temperature is attributed to the change in the temperature of surround structures between measurements. Since this temperature difference does not significantly effect the radiation heat loss at the surface, it is does not appreciably impact the NDE technique, which depends on the thermal time history at a point.

Using a one dimensional model and assuming the time derivative of the temperature is zero, it is possible to estimate that the back side of the panel at the point of

measurement is radiating into an average background temperature of -40°C. As would be expected the temperature is position-dependent, radiating on average into a higher temperature at the base of the panel, where it is closer to the rest of the wing and lower at the apex of the RCC panels, where the heat transfer is dominated by the inner surface of the RCC panel. Since the NDE technique is dominated by the time history at a given point, again these small variations do not significantly impact the NDE technique.

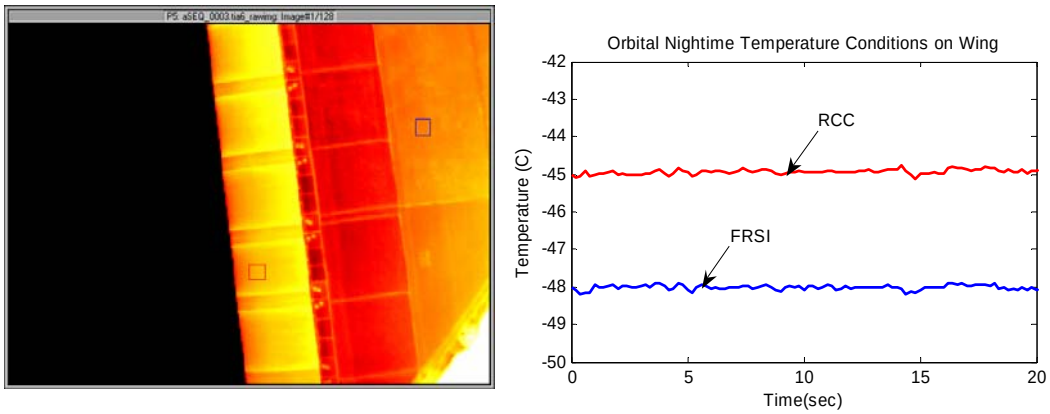

(A) (B)

Figure 9. (A) Infrared image from Shuttle wing leading edge taken at 07:16 CDT on July 15, 2006. Orbital sunrise will occur in approximately 5 minutes. (B) Temperature versus time plots for two regions of the infrared image.

3.2 Objective #2

The second flight test objective was to illustrate the effectiveness of the NDE technique during orbital conditions, validating the ground predictions of the on-orbit system. Four samples of RCC with known defects were flown. Two of these samples were flown in the cargo bay of STS-121 (July 12, 2006), and two were flown in a Test Article Assembly during an International Space Station (ISS) stage EVA (September 15, 2006) conducted between Shuttle flights STS-121 and STS-115. For each of these two flight tests, the two pre-damaged RCC samples included a sample with impact-induced damage and an "NDE Standard" sample. A simple NDE standard with well characterized material variation is fabricated by removing material from the back surface of the sample to specified depths and diameters.

For the samples flown on STS-121 (shown in Figure 10), the NDE standard included flat-bottom holes removing 50% thickness of the material in circular areas with diameters ranging from 2.5 cm. to 5 cm. Diameters of the flat-bottom holes were chosen to approximate delamination sizes of interest to the RCC damage assessment team at the time the samples were fabricated. The sample with impact damage flown on STS-121 had been extensively inspected by both thermography and x-ray CT prior to the flight. This sample was determined to have an approximately 6.3 cm. x 8.1 cm oblong delamination and included a small (1.3 cm long) region of Inner Mold Line (IML) coating loss. No front surface, or Outer Mold Line (OML), damage was present

in either sample. As can be seen in Figure 10c all delaminations and flat bottom holes are clearly visible

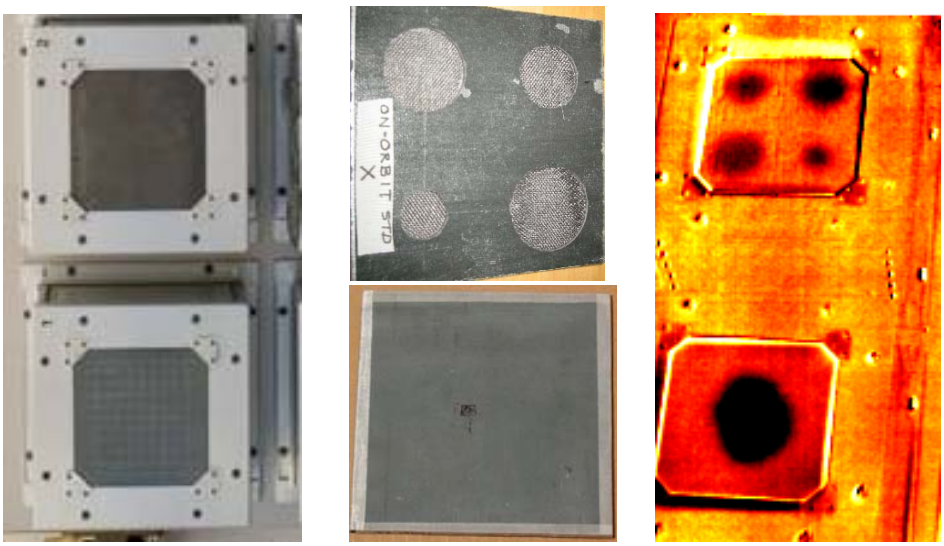

(A) (B) (C)

Figure 10. (A) Photograph of the OML surface of the two RCC samples in the Shuttle cargo bay. No OML surface damage is visible on either sample. (B) Photographs of the IML surface of the same two samples. (C) Processed infrared NDE imagery from STS-121 flight test.

Results for camera tests conducted during the stage EVA on the ISS (Figure 11) resulted in detection of defects approximately 2.5 cm. in diameter created from panel impact and 4 flat-bottom-hole simulated damage regions ranging in size from 2.5 cm in diameter to 5 cm in diameter with 25% material loss from the back surface.

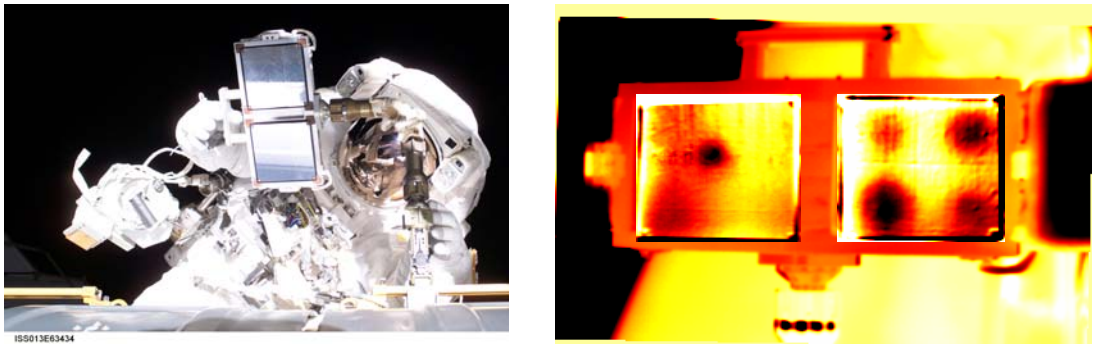

(A) (B)

Figure 11. (A) Astronaut Thomas Reiter prepares the Test Article Assembly for data acquisition. (B) Processed thermal images of acquired data.

4. Conclusions

The EVA IR Camera System has completed three flight tests and has operated successfully each time it has been used in orbit. To date the camera has acquired over 450 Mbytes of on-orbit infrared imagery. All mission objectives have been met, and both the camera and the inspection procedure have been effectively demonstrated. A mature NDE technology for detecting subsurface damage in RCC on the ground has been successfully transitioned and demonstrated as an orbital inspection technique. It has been shown that subsurface delaminations as small as 2.54 cm. in diameter and 75% deep in the RCC panel can be detected with this camera system using passive solar heating. This does not represent the limit of detectability for the system, simply what has been detected to-date.

To minimize the power, weight and cost requirements for the on-orbit system, the EVA IR Camera project team conducted a series of tests on the ground that demonstrated that sunlight and shadowing could be used to create an adequate surface normal thermal gradient in RCC panels. This significantly simplified the development task and reduced project costs. However, it also increases operational complexity, because crewmembers are constrained to inspecting the RCC in sunlight.

References

1. K.E. Cramer and W.P. Winfree, "The Application Of Infrared Thermographic Inspection Techniques To The Space Shuttle Thermal Protection System," Ensayos No Destructivos Y Estructurales, pp. 227-233 (2005).
2. K.E. Cramer, W.P. Winfree, K. Hodges, A. Koshti, D. Ryan and W.W. Reinhardt, "Status of Thermal NDT of Space Shuttle Materials at NASA," Proc. SPIE Vol. 6205, pp. 1B1-9, Thermosense XXVIII (2006).
3. Michael J. Gazarik, Dave Johnson, Ed Kist, Frank Novak, Charles Antill, David Haakenson, Patricia Howell, John Pandolf, Rusty Jenkins, Rusty Yates, Ryan Stephan, Doug Hawk, Michael Amoroso, "Development of an extra-vehicular (EVA) infrared (IR) camera inspection system," Proc. SPIE Vol. 6205, Thermosense XXVIII; Jonathan J. Miles, G. Raymond Peacock, Kathryn M. Knettel; Eds., 2006.
4. N. Rajic, "Principal component thermography for flaw contrast enhancement and flaw depth characterization in composite structures", Composite Structures, Vol. 58, pp. 521-528, 2002.
5. N. Rajic "Principal Component Thermography," DSTO-TR-1298, 2002.
6. W.P. Winfree and J.N. Zalameda, "Thermographic determination of delamination depth in composites", Proc. SPIE Vol. 5073, pp. 363-373, Thermosense XXV, K. Elliott Cramer, Xavier P. Maldague; Eds., 2003.
7. J.N. Zalameda, P.A. Howell and W.P. Winfree, "Compression techniques for improved algorithm computational performance", Proc. SPIE Vol. 5782, pp. 399-406, Thermosense XXVII, G. Raymond Peacock, Douglas D. Burleigh, Jonathan J. Miles; Eds., 2005.
8. Patricia A. Howell and Josepth N. Zalameda, "Computational Analysis for Thermal NDE of Composits," Proc. SPIE Vol. 5191, pp. 18-26, Optical Diagnostics for Fluids, Solids, and Combustion II; Patrick V. Farrell, Fu-Pen Chiang, Carolyn R. Mercer, Gongxin Shen; Eds., 2003.

9. Jahne, Bernd, Practical Handbook on Image Processing for Scientific Applications, CRC Press, New York, 1997.